ELSEVIER

MEMS flow sensors for nano-fluidic applications

Shuyun Wu[*], Qiao Lin, Yin Yuen, Yu-Chong Tai

Caltech Micromachining Laboratory, Electrical Engineering, 136-93, California Institute of Technology, Pasadena, CA 91125, USA

Abstract

This paper presents micromachined thermal sensors for measuring liquid flow rates in the nanoliter-per-minute range. The sensors use a boron-doped polysilicon thin-film heater that is embedded in the silicon nitride wall of a microchannel. The boron doping is chosen to increase the heater's temperature coefficient of resistance within tolerable noise limits, and the microchannel is suspended from the substrate to improve thermal isolation. The sensors have demonstrated a flow rate resolution of 0.4 nl/min, as well as the capability for detecting micro bubbles in the liquid. Heat transfer simulation has also been performed to explain the sensor operation and yielded excellent agreement with experimental data. © 2001 Elsevier Science B.V. All rights reserved.

Keywords: Micro electro mechanical systems; Nano-fluidic applications; Micromachined thermal sensors

1. Introduction

The emerging technology of micro electro mechanical systems (MEMS) is enabling microfluidic systems for many applications, such as micro chromatography, biochemical detection, and mass spectrometry. While precise flow control is generally needed in these applications, existing commercial sensors are inadequate for this purpose because of their limited sensitivity, large size, high dead volume, and difficulties in interfacing with microfluidic devices.

To address the need for precise flow control in microfluidic systems, MEMS technology has been used to develop micro sensors for liquid flow rate measurement [1–4]. Achieving a measuring resolution of up to a few microliters per minute, both thermal [1–3] and non-thermal [4] transducing principles have been used, and channels built using chip-bonding techniques have been employed as the flow-carrying device [1–2].

This paper presents a class of MEMS flow sensors that demonstrate the first capability of measuring liquid flow rates below 20 nl/min at a resolution of approximately 0.4 nl/min, as well as detecting passage of micro bubbles in the flow. These thermal sensors use a boron-doped polysilicon thin-film resistor embedded within the wall of a microchannel. The microchannel, a key feature for our sensors, is fabricated using surface micromachining technology [5] (without chip-bonding), and is released from the

silicon substrate using BrF₃ dry etching [6] for improved thermal isolation. The doping concentration for the polysilicon resistor is optimally chosen for an increased temperature coefficient of resistance, while keeping the noise level within tolerable limits. The subsequent sections describe the design, fabrication, testing, as well as heat transfer analysis of our flow sensors.

2. Design

The basic operating principle of the flow sensor utilizes micro convective heat transfer from a heated polysilicon thin-film sensing element (hereafter referred to as a heater) to a liquid flowing inside a microchannel. Fig. 1 illustrates such a MEMS microchannel flow sensing approach. The polysilicon heater is built on the channel wall. By measuring the sensor temperature, the liquid flow rate can be calculated.

Since the channel is in direct contact with the substrate, the heat loss from the heater to the substrate may considerably reduce the sensor's sensitivity to the fluid flow. Fig. 2 shows an improved approach, in which a portion of the substrate lying below the channel is removed to achieve better thermal isolation. To minimize the effect of channel wall deflection, the heater is located close to the channel outlet.

Since the sensitivity of the sensor also depends on the heater's temperature coefficient of resistance (TCR), we investigated three sensor designs shown in Fig. 3(a)–(c). The microchannels in all three designs have typical

* Corresponding author. Tel.: +1-626-395-8317; fax: +1-626-584-9104.
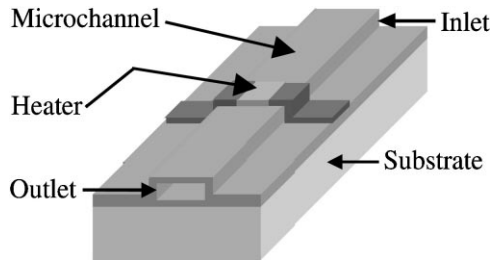*E-mail address*: yctai@mems.caltech.edu (S. Wu).
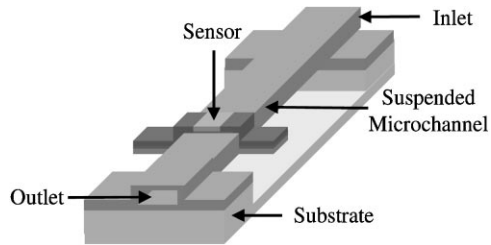
Fig. 1. A microchannel-based flow sensing approach.

Fig. 2. An improved flow sensing approach with a suspended microchannel.

dimensions of $2000 \times 20 \times 2\ \mu m^3$. In the first design (Fig. 3(a)), the microchannel lies directly on the substrate, and the polysilicon heater is heavily doped with boron (concentration $2 \times 10^{19}\ cm^{-3}$). In comparison, the second design as shown in Fig. 3(b), the doping concentration of the polysilicon thin film is reduced to $2 \times 10^{18}\ cm^{-3}$. This increases the heater's TCR (while keeping the noise level within tolerable limits), and hence sensitivity to the flow. Finally, the third design, depicted in Fig. 3(c), employs a
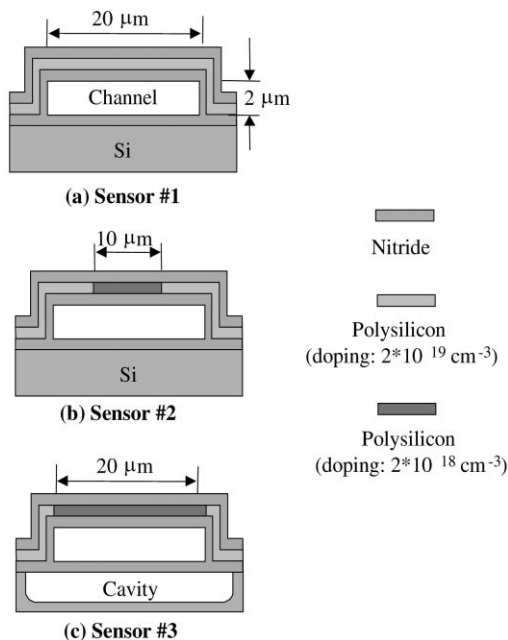
suspended microchannel, which results in improved thermal isolation. Compared with Fig. 3(b), the lightly doped heater length is extended to the channel's entire transverse dimension. This increases the heater's resistance and hence reduces inaccuracies arising from the resistance of the leads and wires. To summarize, these three designs allow us to investigate the effects of channel suspension and heater temperature sensitivity.

3. Fabrication

The fabrication process of the flow sensor, including the microchannel and integrated heating element (Fig. 4), involves the following steps. (1) To start, a $1\ \mu m$ thick silicon nitride layer is deposited onto a bare silicon wafer. (2) A $2\ \mu m$ PSG layer is then deposited on top of silicon nitride. (3) The PSG layer is patterned to define the micro-channel geometry. (4) Anther $0.6\ \mu m$ layer silicon nitride is deposited as the top wall of the microchannel. (5) The PSG is etched away by HF to form the microchannel. (6) Poly-crystalline silicon of $0.5\ \mu m$ is deposited as the sensor material. (7) Polysilicon is doped by B^+ ion implantation, and followed by annealing at $1000°C$ for 30 min. (8) Poly-silicon is patterned by plasma dry etching to define sensor geometry. (9) The sensors are sealed by uniformly depositing $0.6\ \mu m$ of silicon nitride. Then the inlet and outlet are
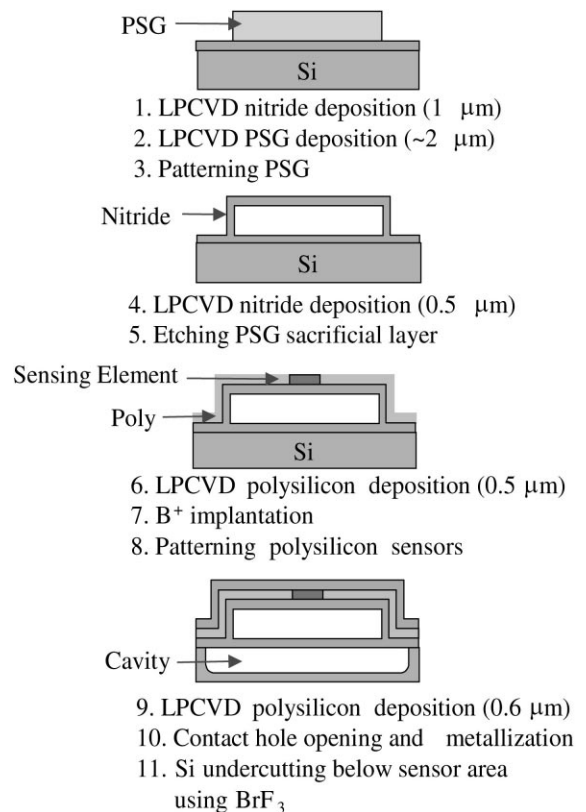

Fig. 3. Three MEMS flow sensor designs.

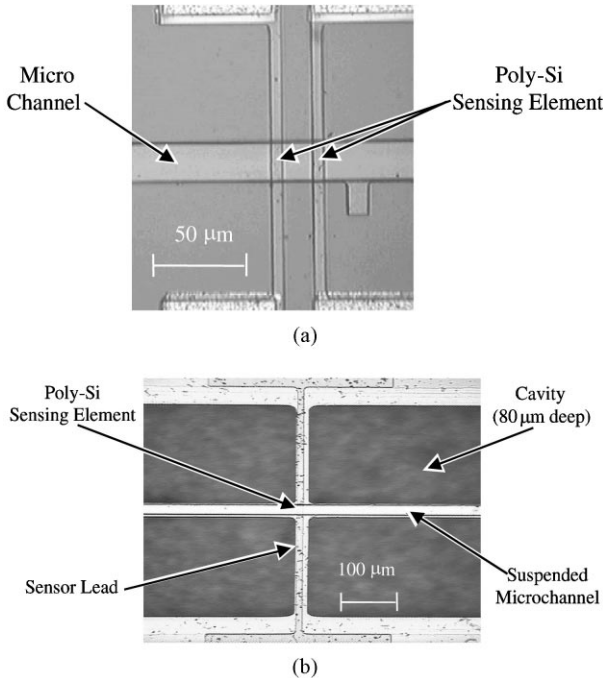Fig. 4. Fabrication process of MEMS flow sensors.

Fig. 5. Fabricated MEMS flow sensors using (a) a microchannel lying on the substrate and (b) a suspended microchannel.

opened by KOH. (10) Contact opening and Al metalization form connections between the macro world and the sensing element. (11) Finally, thermal isolation of the channel is achieved by BrF$_3$ isotropic bulk etching of the silicon underneath the channel.

Fig. 5 shows two fabricated flow sensors. The sensor in Fig. 5(a) is based on a microchannel that lies directly on the substrate, while the sensor in Fig. 5(b) uses a suspended microchannel.

4. Experimental setup

A comparative study was conducted for the three types of flow sensors given in Fig. 3. The package used to perform flow sensor testing is shown in Fig. 6. The sensor chip was glued to an IC package by epoxy, and electrical connection
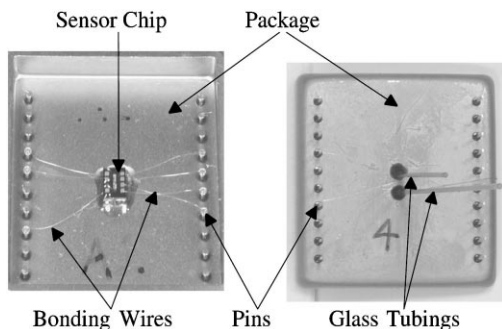

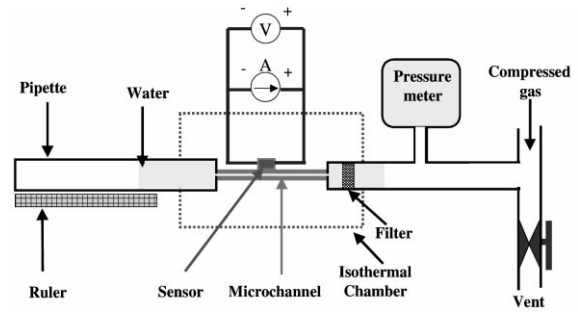Fig. 6. MEMS flow sensor package viewed from the front and back sides.

Fig. 7. Schematic of the calibration system for MEMS flow sensors.

was made by wire bonding. The inlet and outlet of the sensor's microchannel were connected to the macro world by glass tubings.

Fig. 7 shows the setup of our experiment. DI water was forced into the microchannel by pressurized microelectronic grade nitrogen gas from a reservoir tank. The volumetric flow rate was then measured by timing the distance traveled by the water meniscus past marked gradations on a 10 μl glass pipette. Each flow rate data point was taken in a time period between 30 min and 24 h, depending on the flow rate.

The sensor output was taken simultaneously with the flow measurements to give a correlation between sensor readings and flow rate. The sensor was tested and calibrated in an isothermal chamber with ±0.05°C temperature control to minimize ambient temperature fluctuations. The sensors were calibrated against an Omega DP251 Precision Temperature Meter using an RTD probe. With the sensors biased between 70 and 100 μA, the voltage readings were taken using an HP 34970A data acquisition system, thus enabling us to track the time history of sensor readings. The temperature calibration combined with sensor measurements provided thermal data essential for comparison to finite element simulation. Unlike the flow measurements, the sensor measurements were much faster (∼10–60 samples/s) and 100 data points were taken per flow rate measurement.

5. Test results and discussion

We discuss the calibration of the heater resistance as a function of the temperature, the voltage output in response to fluid flow, and flow-induced heater temperature change. Fig. 8 shows the temperature dependence of heater resistance (denoted R) for the three sensors. In the temperature calibration range the resistances decrease linearly with temperature (T), and thus can be characterized as follows.

$$\frac{R(T)}{R(T_0)} = 1 + \alpha(T - T_0) \tag{1}$$

where T_0 is the room temperature and α the temperature coefficient of resistance, or TCR (including the effects of lead and wire resistance change). For sensors 1, 2 and 3, α is found to be -0.17, -0.56 and $-0.67\%/°C$, respectively.

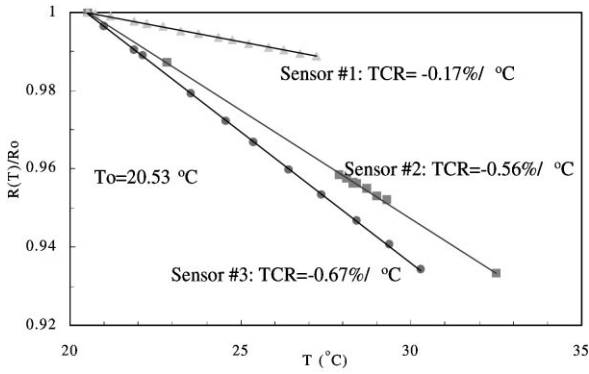Fig. 8. Temperature dependence of resistance for three types of sensors.

Fig. 10. Measured flow-induced temperature change for three types of sensors.

Sensors 2 and 3 have a higher TCR than 1 because of lower doping of the heating region [5]. Compared to sensor 2, sensor 3 has a larger length with lower doping concentration, and hence a slightly higher TCR. According to our calibration, the temperature resolution of all three sensors is better than 0.05°C.

The sensitivity of a sensor, denoted S_V, is defined as the ratio between the changes in output voltage (denoted V) and flow rate (Q), i.e.

$$\Delta V = S_V \Delta Q \tag{2}$$

while S_V varies for different flow rates, the sensitivity can be assessed in an average sense by the slope of a straight line fitted to the measurement data. Fig. 9 shows the measured sensor voltage response to the volumetric flow rate of DI water in the channel under constant current mode, and corresponding fitting lines. We can see that under the same constant current bias at 100 μA, sensor 2 is much more sensitive, Furthermore, even at 70 μA bias current, sensor 3 is 10 times more sensitive to the flow than sensor 2.

Electrically, the output voltage change can be written as

$$\Delta V = I_0[R(T) - R(T_0)] = V_0 \alpha \Delta T, \tag{3}$$

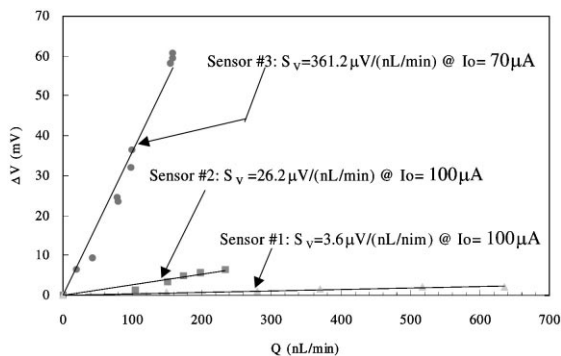where I_0 is the constant current, $V_0 = I_0 R(T_0)$, and $\Delta T = T - T_0$.

From (2) and (3), we have

$$S_V = V_0 \alpha \frac{\Delta T}{\Delta Q} = V_0 \alpha S_T \tag{4}$$

where $S_T \equiv \Delta T / \Delta Q$, called temperature-to-flow ratio, is related to the structure design and fluid properties.

Although S_V is an important sensor characteristic, it involves the original bias voltage that is not related to the sensor design. Thus, it is more appropriate to normalize the sensitivity by the initial bias signal and define the relative sensitivity

$$S_{V/V_0} = \frac{\Delta V/V_0}{\Delta Q} = \alpha \frac{\Delta T}{\Delta Q} = \alpha S_T \tag{5}$$

From Eq. (5), the relative sensitivity is proportional to both the TCR and S_T. Note that the former is related to the sensing material properties and the latter to the sensor configuration design.

Fig. 10 shows the sensor temperature change versus flow rate. We see that for the same given power (140 μW), the suspended flow sensor gives the best temperature-to-flow ratio (0.026°C/nl/min), about five times better than the first two sensors. This indicates that better thermal isolation offered by channel suspension achieves better sensitivity.

Table 1 lists the TCR's, temperature-to-flow ratios and relative sensitivities of the three sensors for an input power of 140 μW. Sensor 3 has the best sensitivity because of its large TCR and temperature-to-flow ratio.

Fig. 9. Measured voltage response of three types of sensors.

Table 1
TCR's, temperature-to-flow ratios and relative sensitivities (input power: 140 μW)

Sensor	1	2	3
α (%/°C)	−0.17	−0.56	−0.67
S_T (°C/nl/min)	0.0047	0.0071	0.0263
S_{V/V_0} (ppm/nl/min)	8	40	180
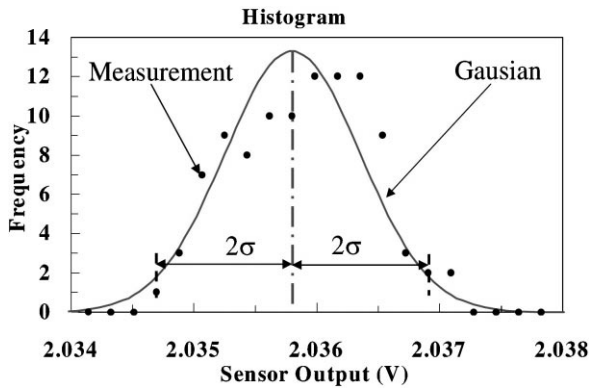
Fig. 11. Histogram of a typical set of sensor measurements.

Fig. 12. Temperature distribution along the channel (sensor 3 at a flow rate of 100 nl/min).

6. Error and resolution analysis

The resolution of the flow sensor is calculated by finding the maximum error associated with the sensor measurements and propagating the error through curve fitting, which gives the flow rate as a function of sensor voltage. It was found that the distribution of voltages for a particular flow rate can be modeled as a two-parameter Guassian distribution. Shown in Fig. 11 is a typical distribution of sensor readings and the fitted Guassian distribution. About 70% of the readings lie within one standard deviation from the mean and 97% within two standard deviations. Thus, two standard deviations were taken as an adequate measure for the maximum error associated with an individual measurement. Further, according to the Central Limit Theorem [7], this error can be reduced by $\sqrt{N}$ through repeated measurements, where N is the number of samples.

Once the errors for each measurement are known, the corresponding error in estimating the flow rate from the calibration can be calculated. For a typical *single* measurement, $2\sigma_V$ is about 1.1 mV, which corresponds to an error in flow rate measurement of about 4 nl/min. Therefore, with 100 repeated measurements, the voltage resolution is $1.1/\sqrt{100} = 0.11$ mV, while the flow rate resolution is given by $4/\sqrt{100} = 0.4$ nl/min.

7. Sensor modeling

To better understand the operation of the flow sensors, the heat transfer occurring in the sensors has been investigated. Note that in this section the term "temperature" will refer to the temperature rise above the room temperature, which, instead of the actual temperature (of the heater, channel or fluid), is used in the simulation.

As a current is passed to the polysilicon heater, heat conduction occurs within the channel's solid structure, including the nitride walls, the embedded polysilicon heater, as well as the surrounding air. This heat conduction is coupled with forced convection heat transfer in the fluid
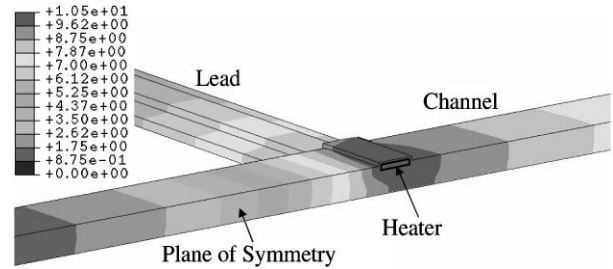
flow. Assuming a laminar incompressible flow, the flow's velocity profile was found analytically [8]. Then, we employed the ABAQUS finite element package to solve the coupled conduction–convection problem, yielding the temperature distribution in both the channel structure and the flow. The average heater temperature for a given flow rate was then computed.

Fig. 12 shows the temperature contours in the flow sensor (sensor 3) at a flow rate of 100 nl/min. It can be seen from this figure that the size of the heated region is comparable along all three spatial dimensions. In contrast to typical macroscale forced convection processes, this implies that heat conduction, in both the channel structure and the flow, in all three spatial directions is equally important for determining the heater's temperature.

Shown in Fig. 13 is the temperature distribution along the microchannel of sensor 3. It can be seen that regardless of the flow rate, the maximum temperature (rise) occurs at the heater location. This should be expected, since the heater is the source of temperature rise in both the channel and the fluid. In addition, the temperature along the channel is symmetric about the heater location when the fluid is stationary, in which case convection is absent and conduction alone determines the temperature distribution. At a
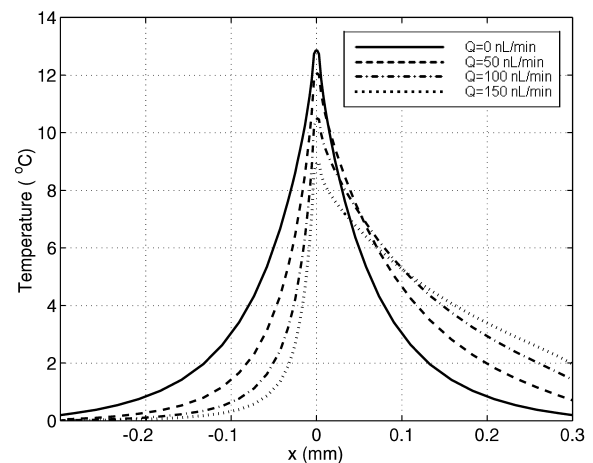

Fig. 13. Temperature distribution along the channel for sensor 3. The *x*-axis is directed along the streamwise direction with the heater at the origin.
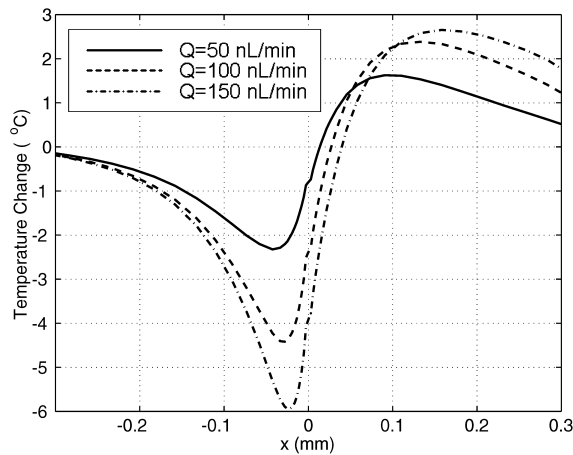
Fig. 14. Distribution of flow-induced temperature change as obtained from data in Fig. 13.

Fig. 16. Real time output of a temperature sensor near the heater of sensor 1. Temperature spikes indicate passage of an air bubble.

nonzero flow rate, forced convection causes heat to be transferred along the flow. As a result, the temperature upstream of the heater decreases, while the temperature downstream of the heater increases. The larger the flow rate, the more significant this flow-induced temperature change.

The temperature at a given point in the microchannel is a function of flow rate, i.e. $T = T(Q)$. Thus, the flow rate information is given by the flow-induced temperature change $\Delta T = T(Q) - T(0)$. The data contained in Fig. 13 can be used to calculate ΔT and the result is shown in Fig. 14. It is very interesting to observe that ΔT generally achieves its maximum away from the heater. Thus, the sensitivity of the flow sensor would be considerably improved if the flow rate is inferred from a separate temperature sensor located at an optimal distance away from the heater. Also, since the temperature change takes on opposite signs upstream and downstream of the heater, use of both upstream and downstream temperature sensors will allow the detection of flow direction.
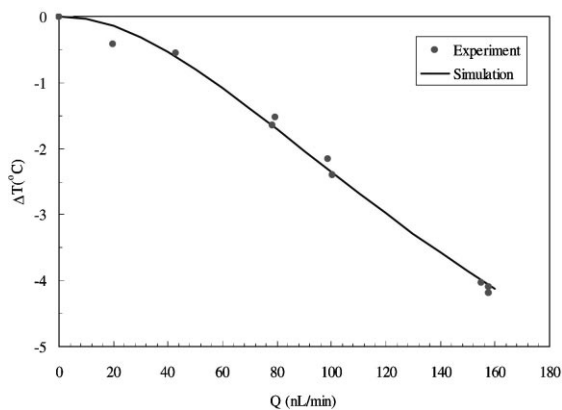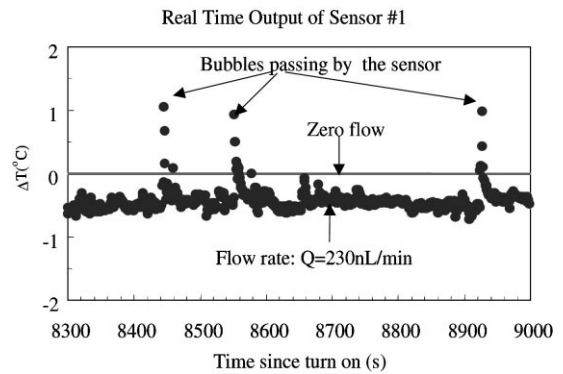
The flow-induced sensor temperature change as a function of flow rate is plotted in Fig. 15 for sensor 3 along with the experimental data. Since there exists considerable uncertainty in the thermal conductivity of silicon nitride, we allow this parameter to be adjusted with respect to the experimental results. The curve in Fig. 15 corresponds to a nitride conductivity of 4 W/m K, which is 25% larger than the nominal value (3.2 W/m K). From the figure we see that when this adjustment is made, there is excellent agreement between simulation and experimental results.

8. Bubble detection

Finally, our flow sensors cannot only measure flow rates, but also detect the presence of air bubbles. In Fig. 16, the passage of air bubbles is logged using real-time data acquisition. In this experiment, one polysilicon element of sensor 1 shown in Fig. 5(a) was used as the heater and the other element as a temperature sensor. Since air has a lower heat capacity and thermal conductivity than water, the temperature sensor sees a sudden temperature rise, shown as spikes in Fig. 16. Further investigation is underway to investigate the possibility of detecting foreign particles other than air bubbles. This can be particularly useful in micro-chemical reaction applications where detection of bubbles or particles is important.

9. Conclusion

We have successfully developed liquid flow sensors that are integrated into a microchannel. The sensor sensitivity can be increased by switching from heavy doping (2×10^{19} cm^{-3}) to relatively light doping (2×10^{18} cm^{-3}), as well as removing a portion of silicon substrate underneath the sensor for better thermal isolation. The flow sensor has demonstrated a resolution of 4 nl/min for single measurement and 0.4 nl/min for averaged multiple measurements. In addition, heat transfer simulation was performed to study the

Fig. 15. Simulated versus measured flow-induced temperature change for sensor 3.

operating principle of the flow sensors, and was found to agree with experimental data. Finally, it was demonstrated that micro bubbles in the liquid flow are detectable by the real time (Fig. 16) recording of sensor output.

Acknowledgements

References

[1] T.S.J. Lammerink, N.R. Tas, M. Elwenspoek, J.H.J. Fluitman, Micro-liquid flow sensor, Sensors and Actuators A 37/38 (1993) 45–50.

[2] T.S.J. Lammerink, V.L. Spiering, M. Elwenspoek, J.H.J. Fluitman, A. van den Berg, Modular concept for fluid handling system: a demonstrator micro analysis system, in: Proceedings of the International Workshop on Micro Electro Mechanical Systems (MEMS'96), San Diego, California, 1996, pp. 389–394.

[3] M. Ashauer, H. Glosch, F. Hedrich, N. Hey, H. Sandmaier, W. Lang, Thermal flow sensor for liquids and gases, in: Proceedings of the International Workshop on Micro Electro Mechanical Systems (MEMS'98), Heidelberg, Germany, 1998, pp. 351–355.

[4] M. Ritcher, M. Wackerle, P. Woias, B. Hillerich, A novel flow sensor with high time resolution based on differential pressure principle, in: Proceedings of the International Conference on Micro Electro Mechanical Systems (MEMS'99), Orlando, Florida, 1999, pp. 118–123.

[5] S. Wu, J. Mai, Y. Zohar, Y.C. Tai, C.M. Ho, A suspended microchannel with integrated temperature sensors for high-pressure flow studies, in: Proceedings of the International Workshop on Micro Electro Mechanical Systems (MEMS'98), Heidelberg, Germany, 1998, pp. 87–92.

[6] X.Q. Wang, X. Yang, K. Walsh, Y.C. Tai, Gas phase silicon etching with bromine triflouride, in: Proceedings of the International Conference on Solid-State Sensors and Actuators (Transducer'97), Chicago, Illinois, 1997, pp. 1505–1508.

[7] G. Casella, R.L. Berger, Statistical Inference, Duxbury Press, 1990, pp. 216–228.

[8] F.M. White, Fluid Mechanics, 2nd Edition, McGraw-Hill, New York, 1986.